Structure and Inhibition of Orotidine 5′-Monophosphate Decarboxylase from *Plasmodium falciparum*[†,‡]

David B. Langley,[§,⊥] Maryam Shojaei,[§,⊥,#] Camilla Chan,[§] Hiu Chuen Lok,[§] Joel P. Mackay,[§] Thomas W. Traut,[△] J. Mitchell Guss,[§] and Richard I. Christopherson*[,§]

School of Molecular and Microbial Biosciences, University of Sydney, Sydney, New South Wales 2006, Australia, and Department of Biochemistry and Biophysics, University of North Carolina, Chapel Hill, North Carolina 27599-7260

Received December 7, 2007; Revised Manuscript Received January 22, 2008

ABSTRACT: Orotidine 5′-monophosphate (OMP) decarboxylase from *Plasmodium falciparum* (*Pf*ODCase, EC 4.1.1.23) has been overexpressed, purified, subjected to kinetic and biochemical analysis, and crystallized. The native enzyme is a homodimer with a subunit molecular mass of 38 kDa. The saturation curve for OMP as a substrate conformed to Michaelis–Menten kinetics with $K_m = 350 \pm 60$ nM and $V_{max} = 2.70 \pm 0.10$ μmol/min/mg protein. Inhibition patterns for nucleoside 5′-monophosphate analogues were linear competitive with respect to OMP with a decreasing potency of inhibition of *Pf*ODCase in the order: pyrazofurin 5′-monophosphate ($K_i = 3.6 \pm 0.7$ nM) > xanthosine 5′-monophosphate (XMP, $K_i = 4.4 \pm 0.7$ nM) > 6-azauridine 5′-monophosphate (AzaUMP, $K_i = 12 \pm 3$ nM) > allopurinol-3-riboside 5′-monophosphate ($K_i = 240 \pm 20$ nM). XMP is an ~150-fold more potent inhibitor of *Pf*ODCase compared with the human enzyme. The structure of *Pf*ODCase was solved in the absence of ligand and displays a classic TIM-barrel fold characteristic of the enzyme. Both the phosphate-binding loop and the $\beta\alpha$5-loop have conformational flexibility, which may be associated with substrate capture and product release along the reaction pathway.

Despite more than a century of efforts to control malaria, the disease remains a major and growing threat to public health. Malaria is caused by four species of the parasitic protozoan genus *Plasmodium*: *P. falciparum*, *P. malariae*, *P. vivax*, and *P. ovale*. Of these species, *P. falciparum* is responsible for most of the 500 million cases of malaria worldwide and for 2–3 million annual deaths (*1, 2*). Biochemical differences between the parasite and host provide a rational basis for the development of antimalarial drugs. One example of this approach is to identify enzymes or metabolic pathways vital for the survival of the parasite that are not essential for the human host. Appropriate enzyme inhibitors could then be developed to block enzymes in these pathways.

The *de novo* pathway for the biosynthesis of pyrimidine nucleotides in *P. falciparum* provides essential precursors for the synthesis of DNA and RNA. Unlike its host, the intraerythrocytic form of the parasite is unable to salvage preformed pyrimidines from its environment and must synthesize pyrimidine nucleotides *de novo* (*3, 4*). As the mature human erythrocyte lacks the *de novo* pyrimidine pathway (*5*), blockade of this pathway could lead to selective death of the intraerythrocytic parasite. The pathway comprises 6 enzyme-catalyzed reactions, the last catalyzed by orotidine 5′-monophosphate decarboxylase (ODCase[1]). ODCase decarboxylates orotidine 5′-monophosphate (OMP) to uridine 5′-monophosphate (UMP, Figure 1a and b). In prokaryotes and lower eukaryotes (such as yeast and *Plasmodium*), the enzymes catalyzing reactions 5 and 6 exist on separate proteins. In mammals, reactions 1–3 and 5 and 6 are contained on multifunctional enzymes. Reactions 5 and 6 are catalyzed by orotate phosphoribosyltransferase and ODCase, collectively named UMP synthase (*6–9*). ODCases are the most catalytically proficient enzymes known, enhancing the rate of reaction by a factor of 10^{17} over the uncatalysed reaction. This rate enhancement is achieved without the aid of metals, cofactors, or the formation of a covalent intermediate (*10, 11*).

Currently, the Protein Data Bank (PDB) contains some 40 ODCase structures from mostly prokaryotic organisms, many deposited by structural genomics consortia and not otherwise published. Organisms whose ODCase structures are accompanied by journal descriptions include *Escherichia coli* (*12, 13*), *Bacillus subtilis* (*14*), *Saccharomyces cerevisiae* (*11, 15, 16*), *Methanobacterium thermoautotrophicum* (comprising almost half the structures, including complexes with UMP, 6-azauridine 5′-monophosphate (AzaUMP, Figure 1c),

[†] This work was supported by the Australian National Health and Medical Research Council, project grant number 253781.

[‡] Refined coordinates and structure factors have been deposited in the Protein Data Bank (entry 2ZCG).

* To whom correspondence should be addressed. Phone: 61-2-9351-6031. Fax: 61-2-9351-4726. E-mail: ric@mmb.usyd.edu.au.

[§] University of Sydney.

[△] University of North Carolina.

[⊥] These authors contributed equally to this work.

[#] Present address: Natural Sciences Department, Tabriz University, Tabriz, Iran.

[1] Abbreviations: AzaUMP, 6-azauridine 5′-monophosphate; ODCase, OMP decarboxylase (EC 4.1.1.23); OMP, orotidine 5′-monophosphate; *Pf*ODCase, ODCase from *Plasmodium falciparum*; PDB, protein data bank; BMP, barbiturate 5′-monophosphate; UMP, uridine 5′-monophosphate; XMP, xanthosine 5′-monophosphate.

10.1021/bi702390k CCC: $40.75
Published on Web 02/28/2008

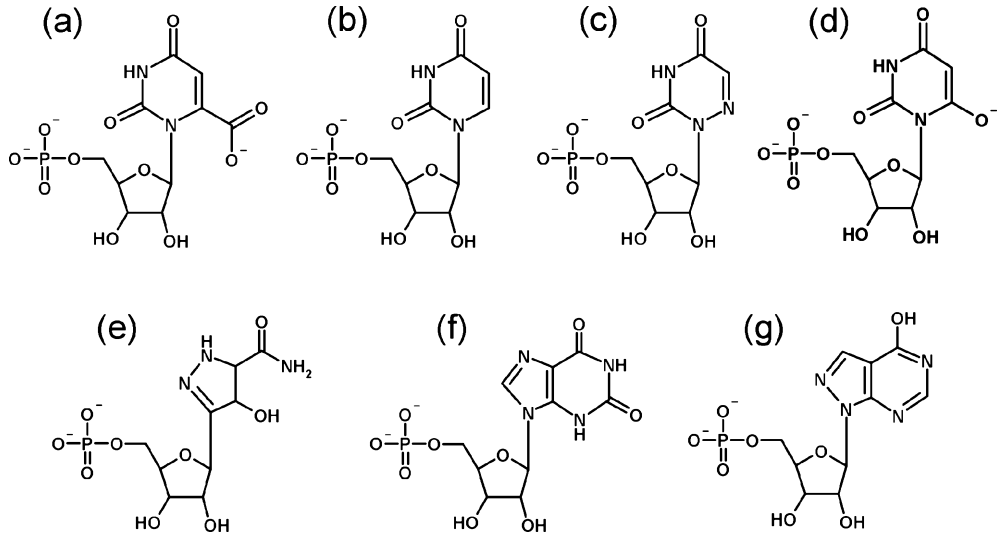

FIGURE 1: Chemical structures of (a) OMP, (b) UMP, (c) AzaUMP, (d) BMP, (e) Pyrazofurin 5′-monophosphate, (f) XMP, and (g) allopurinol-3-riboside 5′-monophosphate.

barbiturate 5′-monophosphate (BMP, Figure 1d) and xanthosine 5′-monophosphate (XMP, Figure 1f)) (*17–20*), and most recently *Plasmodium falciparum*[2]. ODCase structures released prior to publication include those from *Thermatoga maritima* (1 structure, PDB code 1VQT); *Pyrococcus horikoshii* (3 structures, 2CZD, 2CZE, and 2CZF, the latter containing XMP); the pathogenic malarial species, *P. yoelii* (1 structure containing selenium-substituted methionine residues, 2AQW), *P. vivax* (2 structures, 2FFC containing UMP and 2GUU containing AzaUMP), *P. berghei* (1 structure, 2FDS), *P. falciparum* (2 structures, 2F84 and 2Q8L); and *Homo sapiens* (4 structures, 2JGY, 2EAW, 2P1F and 2V30, the latter containing UMP). All ODCases are dimers within the crystal, and the active sites contain residues contributed by both subunits. A catalytic tetrad of noncontiguous residues, Asp-Lys-Asp-Lys, is absolutely conserved and forms a chain of alternating charges lining one end of the binding pocket for the aromatic base. The central pair of these residues, positioned directly opposite the C6 position of the UMP product, are particularly important to the catalytic mechanism, which remains undefined despite numerous mechanistic proposals (*11*). In the "electrostatic stress mechanism" (*19*), for example, the juxtaposition of the carboxylate of OMP with the central aspartate of the Asp-Lys-Asp-Lys motif might lead to destabilization and loss of the carboxylate moiety. The central lysine might facilitate donation of a proton to the resultant carbanion intermediate. Association of OMP with the active site is probably initiated by capture of the phosphoribosyl group. Once tethered, the carboxylated pyrimidine ring is delivered into the narrow active-site cleft, despite likely charge–charge repulsion. Such a combination of both attractive and repulsive forces in a catalytic mechanism has been dubbed the Circe effect (*21*). For comprehensive reviews see Miller and Wolfenden (*11*) and Wu and Pai (*18*).

With a view toward developing potent inhibitors specific to the ODCase of *P. falciparum*, the enzyme was overexpressed in *E. coli*, purified to homogeneity, and characterized. ODCases are known to be inhibited by a number of nucleoside 5′-monophosphate analogues (*22*). Inhibitory properties were determined for some of these analogues; Pyrazofurin 5′-monophosphate (Figure 1e), allopurinol-3-riboside 5′-monophosphate (Figure 1g), AzaUMP, and XMP. Interestingly, XMP proved to be a potent inhibitor of the *Pf*ODCase enzyme ($K_i = 4.4 \pm 0.7$ nM), binding ~150-fold more tightly to the parasitic enzyme than to the human enzyme. A single crystal of *Pf*ODCase was obtained and X-ray diffraction data collected. The structure of *Pf*ODCase, phased from a *P. falciparum* ODCase structure in the PDB (PDB code 2F84), reveals differences that suggest this structure is likely to be a more active enzyme conformation, while the pre-existing structure represents a fold more likely to correspond to a resting or ground-state conformation of the enzyme. Such conformational dynamics are discussed in relation to ODCase structures available from other organisms.

EXPERIMENTAL PROCEDURES

Overexpression and Purification of Recombinant PfODCase. Competent *E. coli* was cotransformed with the plasmids pMICO (*23*) and pET3d-ODC3 (*24*), that carry rare tRNAs and *Pf*ODCase, respectively. Cultures containing ampicillin (100 μg/mL) and chloramphenicol (50 μg/mL) were grown in Luria–Bertani broth at 37 °C until an optical density of 1.8 (600 nm) was reached, after which the temperature was reduced to 25 °C, and the cells were induced with isopropyl β-D-thiogalactopyranoside (IPTG, 250 μM) for 16 h. Post harvest, cells were lysed in buffer containing 50 mM tris-hydroxymethyl aminomethane (Tris)-HCl, 100 mM NaCl, and 10% glycerol at pH 8.0 (Buffer A). After centrifugation (39,000*g*, 30 min, 4 °C), the soluble fraction was loaded onto a Ni-NTA-agarose column (1 × 5 cm, Qiagen) equilibrated with Buffer A containing 300 mM NaCl and 10 mM imidazole. After an additional wash containing 20 mM imidazole, *Pf*ODCase was eluted with running buffer containing 300 mM imidazole. The polyhistidine tag was removed with thrombin (0.06 units/mg protein, Roche) in Buffer A containing 200 mM NaCl, 5 mM imidazole, 5 mM $CaCl_2$ at pH 8.5, at 4 °C overnight. Cleaved *Pf*ODCase was

[2] A brief description of low-resolution structures of *P. falciparum* ODCase (PDB codes 2ZA1, 2ZA2, and 2ZA3) was recently published (*42*) and is discussed further in footnote 3.

then passed over Ni-NTA-agarose resin (collected as the flow-through fraction) and stored in 20 mM Tris-HCl, 10% glycerol at pH 8.0. Cleaved *Pf*ODCase (3 mg) was further purified on a BioCAD chromatography system (GMI, Ramsey, MN) using a POROS-HS cation exchange column (4.6 × 100 mm, GMI) equilibrated with 50 mM 2-(*N*-morpholino)ethanesulfonic acid (MES) and 10% glycerol at pH 6.8, and eluted with a linear gradient of 0–1 M NaCl. The *Pf*ODCase was further purified as a single peak on a Superdex-200 size-exclusion column (1 × 40 cm) eluted with 25 mM 4-(2-hydroxyethyl)piperazine-1-ethanesulfonic acid (HEPES), 150 mM NaCl, 10% glycerol, and 5 mM dithiothrietol (DTT) at pH 7.2. The approximate molecular weight of the peak was determined with a miniDawn multiangle laser light-scatterer (MALLS, Wyatt Technologies, Santa Barbara, CA). The identities of both histidine-tagged and untagged *Pf*ODCase were confirmed by electrospray ionization mass spectrometry using a LCQ Classic mass spectrometer (Thermoquest, San Jose, CA). Protein concentrations were determined using the method of Bradford (*25*) (Bio-Rad), and fractions were analyzed by SDS−PAGE.

Enzymic Synthesis of [2-^{14}C]OMP. [2-^{14}C]OMP was synthesized using a modification of the method of Rawls (*26*). The reaction mixture contained [2-^{14}C]orotic acid (1.20 mM, 55 Ci/mol, Moravek Biochemicals, Brea, CA), 20 units/mL of OMP pyrophosphorylase (Sigma-Aldrich), 20 units/mL of yeast inorganic pyrophosphatase (Sigma-Aldrich), 7 mM 2-mercaptoethanol, 53 mM Tris-HCl (pH 8.0), 5.3 mM $MgSO_4$, and 22.8 mM 5-phosphoriboribosyl-1-pyrophosphate (Sigma-Aldrich) in a total volume of 25 μL. The reaction was incubated at 37 °C for 30 min, terminated by the addition of 0.2 M ice-cold perchloric acid, and neutralized with 2 volumes of organic base (7.7 parts chloroform:2.3 parts trioctylamine). The mixture was centrifuged, and the upper aqueous phase was collected and chromatographed on a Partisil 10-SAX column (250 × 4.60 mm, 10 μm, Phenomenex, Torrance, CA) equilibrated with 50 mM ammonium formate (pH 3.0). [2-^{14}C]OMP was eluted with a linear gradient of 0.1–1 M ammonium formate (pH 3.0) and fractions that absorbed at 275 nm were pooled. The ammonium formate was removed by chromatography on Dowex 50 × 8 resin (100–200 mesh, hydrogen form, Sigma-Aldrich). The yield of [2-^{14}C]OMP was determined using a Typhoon 8600 Variable Mode Imager (Molecular Dynamics, Sunnyvale, CA) with dilutions of standard [2-^{14}C]orotate and the unknown [2-^{14}C]OMP. The ^{14}C-labeled spots on poly(ethylene)imine-cellulose thin layer chromatograms were quantified using ImageQuant software (Molecular Dynamics).

Synthesis and Purification of Nucleoside 5′-monophosphate Analogues. The procedure for the phosphorylation of 6-azauridine at the 5′-position was adapted from Fyfe et al. (*27*). 6-Azauridine (20 mM, Sigma-Aldrich) was incubated with *p*-nitrophenyl phosphate (250 mM), phosphotransferase (partially purified from *Serratia marcescens*; 0.5 mg protein per 1 mL of reaction mixture), and sodium acetate (300 mM, pH 5.0) at 37 °C for 7 days. The reaction was terminated by the addition of ice-cold perchloric acid (0.2 M) and the mixture centrifuged. The supernatant was neutralized with an equal volume of organic base (trioctylamine/freon) and centrifuged. The upper aqueous phase containing the nucleoside 5′-monophosphate was analyzed by thin layer chromatography on poly(ethylene)imine-cellulose with 0.4 M LiCl and 0.1% formic acid. AzaUMP was purified from the phosphotransferase reaction mixture by a procedure modified from Brusilow and Hauser (*28*). The mixture was chromatographed on a Partisil 10-SAX column (Phenomenex) equilibrated with 0.08% formic acid and 35% methanol at pH 2.8, and eluted with a linear gradient from 0 to 1 M ammonium formate (pH 3.0). Synthesis and purification of allopurinol-3-riboside 5′-monophosphate and Pyrazofurin 5′-monophosphate from reaction mixtures were as for AzaUMP.

Assay of PfODCase. Assay mixtures containing 25 mM 3-(*N*-morpholino)-propanesulfonic acid (MOPS), 5% glycerol (pH 7.2), and different concentrations of [2-^{14}C]OMP were preincubated at 37 °C for 5 min, and reactions were started by the addition of 33 pg of pure cleaved *Pf*ODCase. K_m and V_{max} values were determined by measurement of initial reaction velocities in duplicate with at least 8 OMP concentrations. Samples (6 μL) of the assay mixture were taken at three times and spotted onto poly(ethylene)imine-cellulose thin layer chromatograms. ^{14}C-labeled UMP was separated from OMP by ascending chromatography with 0.3 M LiCl and 1% (v/v) formic acid at 4 °C. ^{14}C-labeled OMP and UMP were quantified with a Typhoon 8600 Variable Mode Imager using ImageQuant software (Molecular Dynamics). This sensitive radioassay enabled true initial reaction velocities to be determined with less than 5% conversion of [2-^{14}C]OMP to [2-^{14}C]UMP. The recombinant *Pf*ODCase was stored in 20 mM Tris-HCl and 10% glycerol at pH 8.0, in small aliquots at –80 °C. For each experiment, a fresh aliquot was thawed and diluted just before use. With these precautions, the enzyme was stable for the duration of the assay (20 min) and gave reproducible reaction velocities.

Inhibition Patterns for Nucleoside 5′-monophosphate Analogues. The initial reaction velocities for *Pf*ODCase were determined at 5 concentrations of both inhibitor and [2-^{14}C]OMP. Inhibitors assayed were AzaUMP, allopurinol-3-riboside 5′-monophosphate, Pyrazofurin 5′-monophosphate, XMP (Sigma-Aldrich), and barbiturate riboside 5′-monophosphate (BMP, a gift from Dr. L. Kotra, University of Toronto). The kinetic data obtained were used to construct double reciprocal plots of $1/v$ versus 1/[OMP] at different concentrations of each inhibitor. Initial velocity experiments were carried out in 50 mM MOPS, 150 mM NaCl, and 5% glycerol at pH 7.2. Kinetic data were fitted by nonlinear regression using SigmaPlot (Systat Software Inc., San Jose, CA) to eq 1 describing competitive inhibition:

$$v = V_{max}[\mathrm{OMP}]/((1 + [\mathrm{I}]/K_i)K_m + [\mathrm{OMP}]) \qquad (1)$$

where v is the measured initial rate of reaction, V_{max} is the maximal rate, OMP is the substrate concentration, I is the concentration of the nucleoside 5′-monophosphate analogue, K_m is the dissociation constant for OMP, and K_i is the inhibition constant.

Crystallization and Collection of X-ray Diffraction Data. A single crystal of *Pf*ODCase was grown by the hanging-drop vapor diffusion method whereby an equal volume of protein solution (*Pf*ODCase at 10 mg/mL in 25 mM HEPES (pH 7.0), 150 mM sodium chloride, and 5 mM DTT) was combined with an equal volume of well solution (100 mM sodium acetate (pH 4.6) and 2 M sodium formate). A lone crystal was observed after a two-year incubation at room temperature. The crystal was snap frozen in a stream of

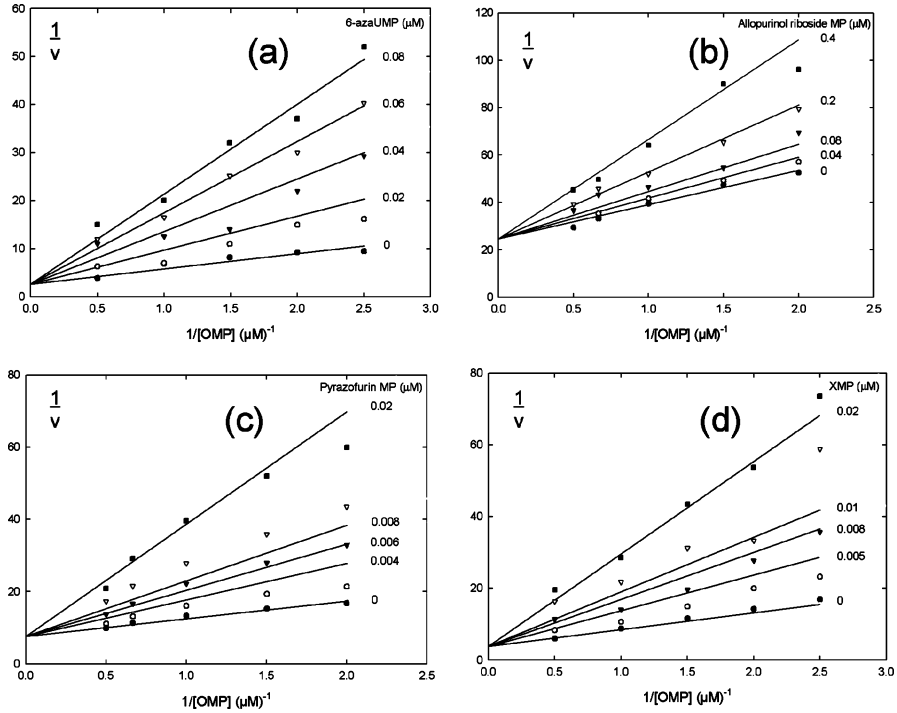

FIGURE 2: Inhibition patterns for nucleoside 5′-monophosphate analogues. (a) AzaUMP, (b) allopurinol-3-riboside 5′-monophosphate, (c) Pyrazofurin 5′-monophosphate, and (d) XMP. Data were fitted to eq 1, and the intersecting lines were generated using the fitted parameters. The K_i values obtained are listed in Table 1. Assays were initiated with 33 pg of *Pf*ODCase as described in Experimental Procedures. Reaction velocity units are pmol/min.

nitrogen vapor at 100 K without any prior cryoprotection regime. Diffraction data were recorded in-house on a Mar345 image-plate detector (Marresearch) using Cu K_α X-rays (λ = 1.5418 Å) from a Rigaku RU-200 rotating anode generator with Osmic mirror optics (both Rigaku). Reflections were indexed and scaled using the HKL software suite (*29*).

X-ray Structure Refinement. The structure was solved by molecular replacement using the program MOLREP (*30*), part of the CCP4 suite of crystallographic software. The search model comprised the *Pf*ODCase structure already in the PDB (PDB code 2F84) stripped of solvent molecules and phosphate ions. An initial low-resolution round of rigid-body refinement was followed by multiple rounds of restrained *B*-factor refinement using REFMAC5 (*31*). Between rounds of refinement, the model was manually inspected and adjusted in conjunction with electron density maps using COOT (*32*). Solvent molecules were added if warranted by sufficient electron density and sensible geometry. Calculation of the buried dimerization surface was performed with areaIMOL (*33*). Structure validation was performed using the MOLPROBITY server (*34*).

RESULTS

Characterization of Recombinant PfODCase. SDS−PAGE analysis of purified *Pf*ODCase showed a single band with a molecular mass of ~38 kDa. Size-exclusion chromatography coupled to a MALLS detector gave a molecular mass for the enzyme particle of ~76 kDa (data not shown) consistent with a homodimer; the molecular mass of the tagless monomer was calculated to be 37.8 kDa. Analytical ultracentrifugation confirmed the enzyme to be dimeric in solution with an estimated weight-average molecular mass of 66–80 kDa (data not shown).

Table 1: Inhibition of ODCases

substrate or inhibitor	apparent K_m or K_i (nM) *P. falciparum*[a]	*H. sapiens*	*S. cerevisiae*	Hs/Pf	Sc/Pf
OMP	350 ± 60	295[b]	700[f]	0.84	2.0
UMP		24000[c]	200,000[f]		
AzaUMP	12 ± 3	510[c]	64[f]	43	5.3
Allopurinol-MP	240 ± 20	2600[d]	1000[d]	11	4.2
BMP		0.009[c]	0.009[g]		
Pyrazofurin-MP	3.6 ± 0.7		5[e]	0.28	1.4
XMP	4.4 ± 0.7	670[c]	410[f]	150	93

[a] From Figure 2. [b] Yablonski et al. (1996) (*9*). [c] Miller et al. (1998) (*38*). [d] Brown and O'Sullivan (1977) (*37*). [e] Dix et al. (1979) (*39*). [f] Miller and Wolfenden (2002) (*11*). [g] Levine et al. (1980) (*41*).

Kinetic Analysis of Inhibitors of PfODCase. K_m and V_{max} values of *Pf*ODCase for OMP were determined by measurement of initial reaction velocities in duplicate at 8 concentrations of [^{14}C]OMP to give V_{max} = 2.7 ± 0.10 μmol/min/mg protein, and K_m^{OMP} = 350 ± 60 nM. A pH-rate (V_{max}) curve determined for *Pf*ODCase from pH 4.5–9.0 showed an optimum at pH 7.3 in buffer containing 5% glycerol and 150 mM NaCl. The enzyme is susceptible to dilution inactivation and was stabilized with glycerol (5–10% v/v) and NaCl (150 mM) in purification and storage buffers. Inhibition patterns intersecting on the ordinate, consistent with competitive inhibition, were obtained for AzaUMP, allopurinol-3-riboside 5′-monophosphate, Pyrazofurin 5′-monophosphate, XMP, and BMP. Data for all inhibitors except BMP were linear competitive with respect to OMP (Figure 2) and were fitted by nonlinear regression to eq 1 to determine the kinetic parameters (Table 1). The nucleoside 5′-monophosphate analogues showed a decreasing potency of inhibition of *Pf*ODCase in the order: Pyrazofurin 5′-monophosphate (K_i = 3.6 ± 0.7 nM) > XMP (K_i = 4.4 ± 0.7 nM) > AzaUMP (K_i = 12 ± 3 nM) > allopurinol-3-

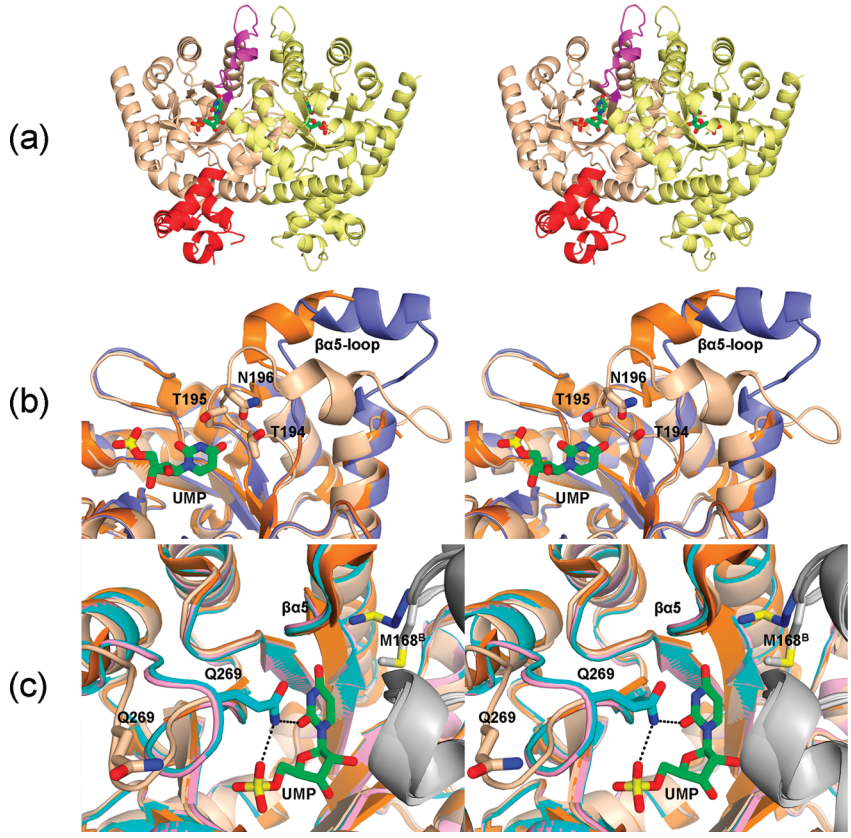

FIGURE 3: Structures of malarial ODCases. (a) *Pf*ODCase dimer with one subunit colored yellow and the other tan. The $\beta\alpha5$-loop (magenta) and $\beta\alpha1$-loop (red) are highlighted. The active sites are indicated by stick representations of UMP superposed from the *P. vivax* structure (PDB code 2FFC). (b) Different *Pf*ODCase conformations. *Pf*ODCase solved in this work (tan) is superposed with other malarial structures differing in the position of the $\beta\alpha5$-loops (blue, PDB code 2F84; orange, PDB code 2Q8L). Labeled residues and superposed UMP are shown as sticks. (c) Superposed ODCases from *P. falciparum* (tan), *P. vivax* (cyan), *P. yoelii* (pink), and *P. berghei* (orange). All B-subunits are colored gray. Q269 (sticks) projects from the phosphate-binding loop (closed for *P. vivax*, open for *P. falciparum*). UMP is from the *P. vivax* structure. $M168^B$ is shown in two conformations (sticks), corresponding to active- (gray) and resting-$\beta\alpha5$-loop (blue) *Pf*ODCase conformations.

riboside 5′-monophosphate ($K_i = 240 \pm 20$ nM). The results of Figure 2 summarized in Table 1 indicate that all inhibitors bind more tightly to *Pf*ODCase than the substrate OMP. The potent inhibitor BMP, showed complex nonlinear kinetics, and data were not fitted to a velocity equation describing inhibition (Shojaei, M, Kotra, L., and Christopherson, R. I., data not shown).

Global Fold of Malarial ODCases. The structures of ODCases from *P. falciparum*, *P. vivax*, *P. yoelii*, and *P. berghei* are relatively recent additions to the PDB. All four have the canonical $(\beta\alpha)_8$ TIM-barrel fold typical of the enzyme, with the active site sitting at the C-terminal end of the β-strands forming the barrel (Figure 3a). In each case, the α-helical components connecting the β-strands of the TIM-barrel are well defined. All crystallize as dimers, with the active site partially formed by the dimer interface. The folds of the *P. vivax*, *P. yoelii*, and *P. berghei* structures superpose well across nearly the entire length of the protein, regardless of the presence or absence of a ligand in the active site. In contrast, the *P. falciparum* structures (PDB codes 2F84 and 2Q8L), although similar to the other malarial species, adopt a distinctly different fold starting at the C-terminus of the $\beta5$ sheet and extending into the $\beta\alpha5$-loop that contributes to the dimerization surface (Figure 3a, magenta ribbon).

Open and Closed $\beta5$-Strand and $\beta\alpha5$-Loop Conformations. Crystallographic and refinement statistics for our *Pf*ODCase structure are presented in Table 2. Despite the resolution of this structure being modest (2.2 Å), all active site residues are well defined by the electron density and are unambiguously modeled. The two subunits of the dimer present in the asymmetric unit are essentially identical (root-mean-square deviation ~0.39 Å for 314 CA positions, Table 3). The fold of our *Pf*ODCase (Figure 3a) closely resembles the structures from the other species of *Plasmodium* with the $\beta5$ strand positioned such that residues T194, T195, and N196 form one end of the active site pocket (Figure 3a, magenta ribbon and Figure 3b, tan ribbons and sticks). Hence, with respect to the conformation of the $\beta\alpha5$-loop, we refer to our structure of *Pf*ODCase as the active conformation of the enzyme (*Pf*ODCase-act). When superposed with the *Pf*ODCase structures 2F84 and 2Q8L, residues 192–212 that constitute the C-terminal end of the $\beta5$-strand and the $\beta\alpha5$-loop adopt a different peptide backbone path (Figure 3b, blue and orange ribbons, respectively). The 2Q8L and 2F84 structures share the same peptide backbone fold until T195, where they also diverge to follow distinct paths. In both conformations, residues that would normally line the active site cavity are withdrawn, resulting in the active site pocket being considerably more open. Hence, with respect to the $\beta\alpha5$-loop, these structures may represent resting or ground-state conformations of the enzyme (*Pf*ODCase-rest). The conformational flexibility inherent in this region is exemplified by residues 204–210

Table 2: X-ray Data Collection and Refinement Statistics for *Pf*ODCase-act

wavelength (Å)	1.5418
space group	$P2_1$
unit cell dimensions: *a*, *b*, *c* (Å); β (°)	60.9, 104.1, 62.4; 113.8
molecules per asymmetric unit	2 (forming one ODCase dimer)
resolution range (Å)	15.01 – 2.22
no. of unique reflections	32849
completeness (%)	99.0 (95.4)[a]
redundancy	4.3 (3.0)[a]
average *I*/Sig(*I*)	9.6 (3.2)[a]
R_{merge}[b]	0.102 (0.319)[a]
Wilson *B* value (Å^2)	25.2
no. of non-H atoms	5296
residues modeled at occupancy = 1.00	A2-A72, A75-A321 B2-B71, B75-B268, B272-B322
residues modeled at occupancy = 0.01	A40, A52, A209, A210 B209, B210
water molecules	80
RMSD bond lengths (Å)	0.012
RMSD bond angles (°)	1.27
R.MSD peptide planarity (°)	6.30
Ramachandran - Favored regions (%)[c]	97.1
Ramachandran - outlier regions (%)[c]	0.32 (residues A109 and B210)
ESU (Å), based on max likelihood[d]	0.164
Mean B (Å^2)	37.6
R[e]	0.201 (0.198)[a]
R_{free}[f]	0.271 (0.318)[a]
PDB identifier	2ZCG

[a] The values in parentheses are for the highest resolution shell (2.28–2.22 Å). [b] $R_{merge} = \Sigma|I_h - \langle I_h\rangle|/\Sigma\langle I_h\rangle$. [c] Calculated using the MOLPROBITY server. [d] Diffraction-component precision index output by REFMAC5. [e] R values $= \Sigma|F_{obs} - F_{calc}|/\Sigma F_{obs}$. [f] Five percent of the reflections were reserved for the calculation of R_{free}.

being unresolved in the 2Q8L structure. Additionally, the side chain of a methionine residue that projects from the dimer partner into the active site pocket ($M168^B$) is positioned differently in the *Pf*ODCase-rest structures (Figure 3c, carbons as blue sticks).

The $\beta\alpha5$-loop, observed in multiple conformations in *Pf*ODCase structures, also contributes to the dimer interface where it interacts with the analogous component from the other subunit of the dimer, bisected by either a noncrystallographic 2-fold axis (our structure, with a dimer in the asymmetric unit) or by a crystallographic 2-fold axis (2F84 and 2Q8L, with monomers in the asymmetric unit; Table 3). The different arrangements of this loop are reflected in the different monomer–dimerization surfaces calculated totaling ~2400, ~1900, and ~1600 Å^2 for the *Pf*ODCase-act, 2F84, and 2Q8L structures, respectively. However, the smaller buried surfaces for the 2F84 and 2Q8L structures are somewhat compensated by different crystal contacts existing in these structures (which share the same space group and unit cell dimensions), where the tip of the C-terminal helix from a nondimer molecule substitutes for surface normally contributed by the $\beta\alpha5$-loop (Supporting Information, Figure S1). This crystal contact is absent in the *Pf*ODCase-act structure. The *Pf*ODCase-rest structures have a phosphate ion at the phosphate binding site, located at the opposite end of the active site with respect to the $\beta5$-strand and $\beta\alpha5$-loop. Although our *Pf*ODCase-act structure lacks phosphate, the surrounding residues are identically positioned.

Active Sites of the Malarial Enzymes. The homology of amino acid sequences between the four malarial ODCases is high (Table 3), and the residues proposed to line the active site are conserved (*24, 35*). The structure is also conserved except for the conformation of the $\beta\alpha5$-loops of the *Pf*ODCase-rest structures noted above. The *P. vivax* ODCase structures contain either UMP or AzaUMP in essentially identical active-site positions. The *P. yoelii* structure has a sulfate ion occupying the phosphate-binding site, while the *P. berghei* structure has an iodide ion in the aromatic ring-binding half of the active site. The side chain of R294 in the *P. berghei* structure (*P. falciparum* numbering is used for all malarial structures), expected to hydrogen bond the phosphate group of OMP (Figure 4a), is in a different conformation compared to the other malarial structures. Additionally, residues A268, Q269, and D270, which form the so-called phosphate-binding loop (*19*) are unresolved in the *P. berghei* structure. The conformation of these three residues is conserved in the *P. vivax* and *P. yoelii* structures, with the side chain of Q269 extending into the active site pocket such that the NE2 nitrogen hydrogen-bonds both the O2 carbonyl oxygen of UMP or AzaUMP (*P. vivax* structures) and an oxygen of the 5′-phosphate (or sulfate in the case of the *P. yoelii* structure) (Figure 3c, dashed lines), a closed conformation of the phosphate-binding loop. This loop in the *P. falciparum* structures is oriented in an open conformation (PDB 2F84 and A-subunit of *Pf*ODCase-act, Figure 3c) or is unresolved (PDB 2Q8L and B-subunit of *Pf*ODCase-act). In the A-subunit of *Pf*ODCase-act, the open loop participates in crystal contacts with a nondimer molecule of the crystal lattice (Table 3). The dynamic nature of the phosphate-binding loop might involve substrate capture and product release. Our unliganded *Pf*ODCase-act structure contains well-ordered water molecules in both active sites of the dimer (Figure 4b, red and yellow transparent spheres). Interestingly, although the amino acid side chains of residues directly adjacent to these waters are essentially identically positioned in the two active sites, some of the waters are uniquely positioned. In contrast, solvent molecules occupy predominantly different positions in the *Pf*ODCase-rest structures.

ODCases from Other Organisms. We have compared our *Pf*ODCase structure with ODCases from *H. sapiens*, *S. cerevisiae*, *P. horikoshii*, *M. thermoautotrophicum*, *B. subtilis*, *E. coli*, and *T. maritima* (Table 3). Although available in the PDB, many of these structures are not described in the literature. The human ODCase is of particular interest as differences with *Plasmodium* might be exploited for development of antimalarial drugs. ODCases from *P. horikoshii* (a hyperthermophile archaeon, PDB code 2CZF) and *M. thermoautotrophicum* (PDB code 1LOL) are the only structures containing XMP, shown here to preferentially bind *Pf*ODCase compared with the human enzyme (Table 1). All other ODCases have the same basic dimeric TIM-barrel scaffold described for the malarial enzymes. The malarial enzymes have an additional ~55 residues inserted at the $\beta\alpha1$-loop, which forms an α-helical bundle (Figure 3a, red ribbon). More minor differences concern the size and conformation of the $\beta\alpha5$-loop, which is generally smaller in nonmalarial ODCases, and the size and disposition of the phosphate-binding loop (discussed below).

Table 3: Selected ODCase Structures

organism	PDB code	consortium (group)[c]	reference	% identity to *Pf*ODCase	RMSD[d] (aligned CA atoms)	res (Å)	mol/asu	ligand (chain)[f]	fold (PBL; phosphate-binding loop)	open PBL contributes crystal contacts
P. falciparum	2ZCG	this work	this work	100	0.387 (314)[e]	2.2	2		PBL open (A), unresolved (B)	A-yes; B-no
P. falciparum	2F84	SGPP		100	0.499 (300)	2.1	1	PO_4^{3-}	PBL open, $\beta\alpha5$ resting-x[g]	no
P. falciparum	2Q8L	SGC		100	0.500 (298)	2.1	1	PO_4^{3-}	PBL unresolved, $\beta\alpha5$ resting-y[g]	
P. vivax	2FFC	SGC		65	0.810 (308)	1.7	1	UMP	PBL closed	
P. vivax	2GUU	SGC		65	0.806 (308)	1.86	1	AzaUMP	PBL closed	
P. yoelii	2AQW[b]	SGC		68	0.863 (310)	2.0	1	SO_4^{2-}	PBL closed	
P. berghei	2FDS	SGC		67	0.795 (313)	1.72	2	I^-	PBL unresolved	
H. sapiens	2EAW	(Pai)		20	1.96 (203)	2.88	2	SO_4^{2-} (A only)	PBL closed	
H. sapiens	2P1F	(Pai)		20	1.91 (205)	1.76	1	SO_4^{2-} and glycerol	PBL closed	
H. sapiens	2V30	SGC		19	1.92 (207)	2.0	2	UMP	PBL closed	
H. sapiens	2JGY	SGC		19	2.04 (202)	1.95	2		PBL unres (diff A and B folds)	
S. cerevisiae	1DQX	(Short)	*16*	18	1.89 (203)	2.40	4	BMP	PBL closed	
S. cerevisiae	1DQW	(Short)	*16*	19	2.11 (202)	2.1	4		PBL open	A,C-no; B,D-yes
P. horikoshii	2CZE	RSGI		25	1.61 (195)	1.85	2	UMP	PBL closed	
P. horikoshii	2CZF	RSGI		24	1.94 (195)	1.85	2	XMP-x,y[g]	PBL open-x (A), closed (B)[g]	A-yes
P. horikoshii	2CZD	RSGI		24	1.85 (191)	1.6	2	DTT (A only)	PBL open-y[g]	A-no; B-yes
M. thermoaut.[a]	1LOQ	(Pai)	*17*	21	1.79 (194)	1.5	2	UMP	PBL closed	
M. thermoaut.[a]	1LOL	(Pai)	*17*	18	1.97 (189)	1.9	2	XMP and 1,3-butanediol	PBL unresolved	
M. thermoaut.[a]	1DV7	(Pai)	*19*	19	2.03 (191)	1.8	1		PBL unresolved	
E. coli	1EIX	(Larsen)	*13*	18	2.06 (187)	2.5	4	BMP	PBL closed	
E. coli	1L2U	(Larsen)	*12*	17	2.36 (191)	2.5	2		PBL unresolved	
B. subtilis	1DBT	(Ealick)	*14*	22	2.19 (188)	2.4	3	UMP	PBL closed	
T. maritima	1VQT	JCSG		21	2.73 (178)	2.0	1	2 × 1,2-ethanediol	PBL unresolved	

[a] *M. thermoautotrophicum*. [b] Selenomethionine substituted. [c] SGPP, Structural Genomics of Pathogenic Protozoa Consortium; SGC, Structural Genomics Consortium; RSGI, RIKEN Structural Genomics/Proteomics Initiative; JCSG, Joint Center for Structural Genomics; (Pai), Dr. Emil Pai, University of Toronto; (Short), Dr. Steven Short, Glaxo Wellcome; (Larsen), Dr. Sine Larsen, University of Copenhagen; (Ealick), Dr. Stephen Ealick, Cornell University. [d] Superposition of A-chain onto A-chain of *Pf*ODCase-act. [e] Superposition of B-chain of *Pf*ODCase-act onto A-chain of *Pf*ODCase-act. [f] Chain descriptor only used in case of differences between chains. [g] x and y denote different conformations.

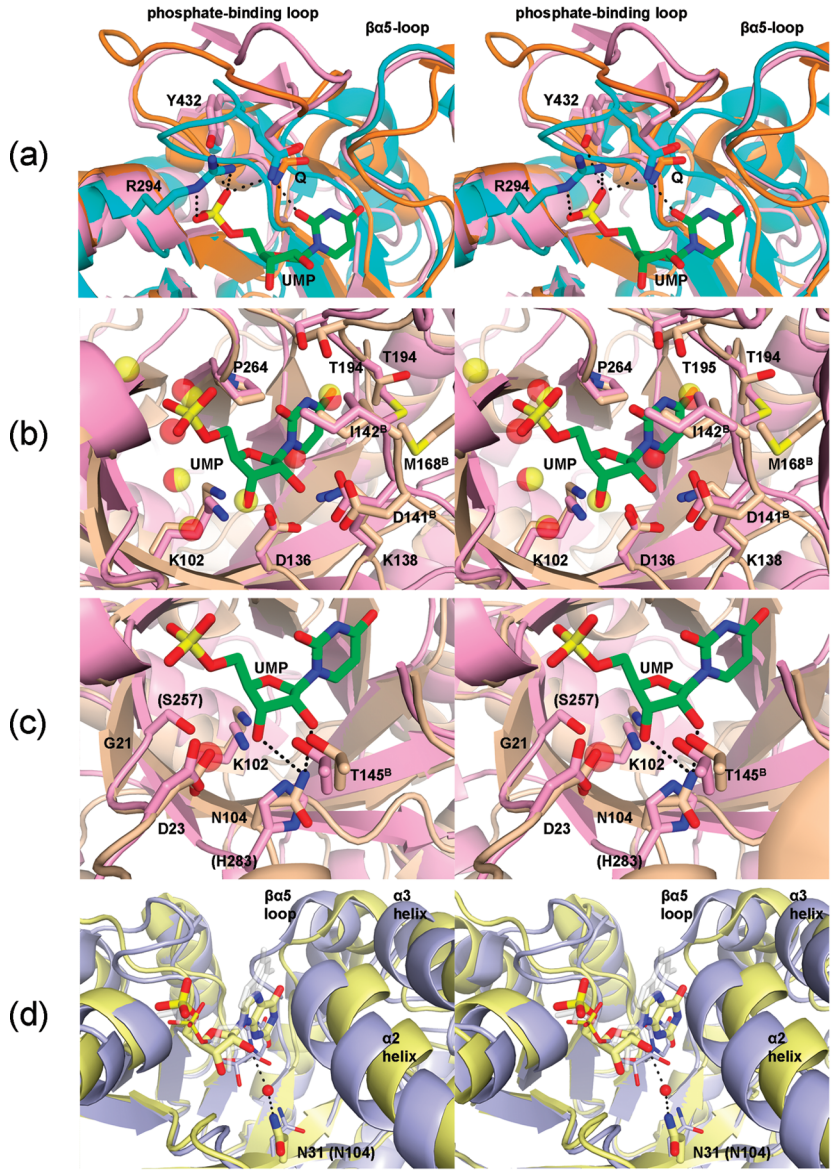

FIGURE 4: Malarial ODCase superposed with enzymes from different species. (a) *P. vivax* ODCase (cyan ribbon and sticks, *Pf*ODCase numbering, and UMP) is superposed with ODCases from human (pink ribbon and sticks) and *B. subtilis* (orange ribbon and sticks), each complexed with UMP. The B-chain of the dimer is omitted for clarity. Hydrogen bonds are shown as dashed lines. (b) Pyrimidine-binding pocket of *Pf*ODCase-act (tan and residue annotation) and human ODCase (pink). The UMP molecule is superposed from a *P. vivax* structure. Water molecules resolved in the A- and B-active sites of *Pf*ODCase-act are represented by red and yellow transparent spheres. (c) Ribose-binding pocket of *Pf*ODCase-act (tan and annotation) and human ODCase (pink and annotation in parentheses). Hydrogen bonds (dashed lines) connect ribose hydroxyls and N104. The water molecule (red transparent sphere) belongs to *Pf*ODCase. (d) ODCase from *P. horikoshii* complexed with either UMP (light-blue ribbon and thin sticks) or XMP (pale-yellow ribbon and thick sticks). Superposed XMP from the B-chain of the dimer is shown as transparent sticks. Hydrogen bonds (dashed lines) via a bridging water (red sphere) connect XMP to N31 (equivalent to N104 in *Pf*ODCase).

Dynamic Loops. The other ODCase structures in the PDB do not show the conformational variability in the βα5-loop noted for *Pf*ODCase. However, conformational variability frequently occurs in the phosphate-binding loop, which constitutes the major difference between ODCase structures (Figure 4a). For example, the *Methanobacterium* enzyme has a phosphate-binding loop similar to that of the malarial enzyme, which is observed in a closed conformation with UMP (PDB code 1LOQ), but is unresolved with XMP (PDB code 1LOL) or without ligand (PDB code 1DV7). The *Pyrococcus* enzyme has a similar loop that is closed with UMP (PDB code 2CZE) and closed or open with XMP at the active site (the crystallographically distinct subunits of the dimer bind XMP differently; PDB code 2CZF). The open conformation for this enzyme, however, is distinct from that observed in the *Pf*ODCase structures (not shown).

The yeast and human enzymes have much larger phosphate-binding loops, which close over the substrate-binding pocket and make more substantial contact with the dimer partner (Figure 4a, pink ribbon). Of the four human ODCase structures available, one contains UMP (PDB code 2V30), and one contains a glycerol molecule within the active-site cleft (PDB code 2P1F). Although the phosphate-binding loop of the human enzyme is larger than that for *Pf*ODCase, its interaction with UMP is similar to that of other ODCases (Figure 4a, pink ribbon and sticks). A glutamine residue

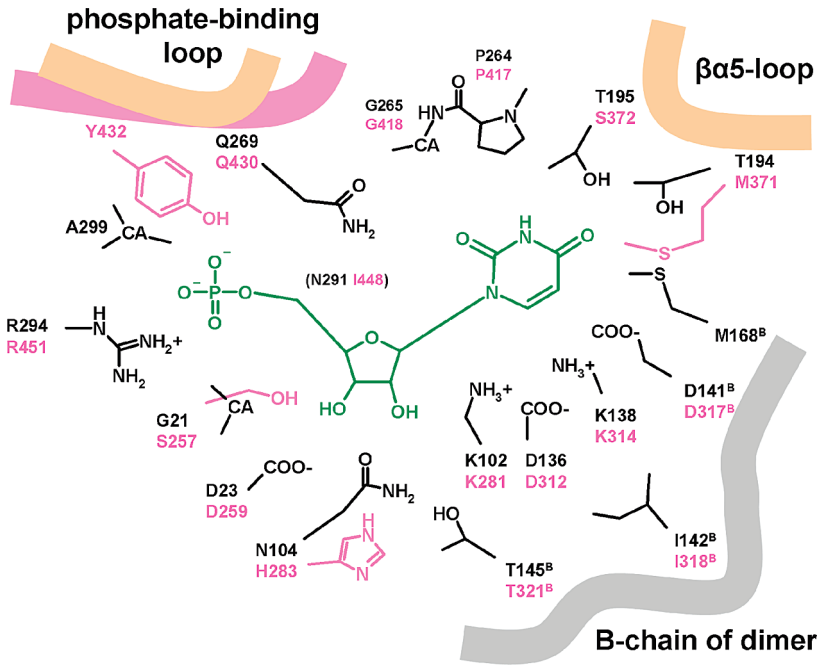

FIGURE 5: Structurally homologous active site residues for malarial and human ODCases (black and pink features, respectively) in close proximity to UMP (green sticks). For clarity, only selected residues are displayed.

(Q430, Q in Figure 4a) projects from the loop to simultaneously hydrogen bond both ends of UMP. The human enzyme also has an additional residue that hydrogen bonds the phosphate group of the substrate (Y432). Structurally analogous residues of *Pf*ODCase and human ODCase are illustrated in Figure 5. The yeast and human enzymes have ~51% identical amino acid sequences and share the same phosphate-binding loop. Of the two yeast structures available, one contains the potent inhibitor BMP at the active site (PDB code 1DQX), with the pyrimidine base occupying the same position as UMP in the human enzyme and the phosphate-binding loops similarly arranged. In the absence of ligand (PDB code 1DQW), the phosphate-binding loop of the yeast enzyme assumes an open resting or ground-state conformation, which contributes crystal contacts to neighboring molecules in the crystal lattice (Table 3).

The *E. coli* and *B. subtilis* structures (41% identical amino acid sequences) have a similarly sized, although conformationally distinct, phosphate-binding loop compared to those of the human and yeast structures. This loop similarly projects a glutamine residue that hydrogen bonds both ends of UMP (Figure 4a, orange ribbon and sticks). When the *E. coli* enzyme is complexed with BMP (PDB code 1EIX), the inhibitor overlays UMP bound in the *B. subtilis* structure (PDB code 1DBT). The glutamine residue makes similar hydrogen bonds with UMP and BMP. For both bacterial ODCases, an arginine substitutes for the tyrosine ligand to the phosphate noted in the human and yeast structures, absent in the malarial structures. In the absence of ligand, the phosphate-binding loop of the *E. coli* structure is unresolved (Table 3).

Environment of the Pyrimidine Ring and Ribose Group. Features conserved between ODCases include the alternating arrangement of charged residues believed to induce decarboxylation (K102, D136, K138, and D141^B projecting from the dimer partner, Figure 4b), and residues that sandwich the pyrimidine ring of substrate or product (P264, I142^B, and T145^B, Figures 4b and 5). A hydrophobic pocket adjacent to the C6 atom of superposed UMP (defined by residues T163, V240, L262, P264, and nonpolar components of N291 and K102) may temporarily accept CO_2 during the catalytic cycle (*19*).

The environment surrounding the ribose group of OMP is conserved except for regions below the 2′- and 3′-hydroxyl groups of the ribose and adjacent to the 3′-hydroxyl (Figure 4c). In the malarial and *Pyrococcus* structures of UMP complexes, the OD1 oxygen of an asparagine residue is positioned to form bifurcated hydrogen bonds with the 2′- and 3′-hydroxyls of the ribose. The analogous residue in the human and yeast structures is histidine (Figures 4c and 5, H283). For the human structures liganded by UMP or glycerol, NE2 of this histidine is modeled to project approximately between the ribose hydroxyls or similarly positioned glycerol hydroxyls. Such a nonideal hydrogen-bonding arrangement may in fact reflect the average of side-chain conformations whereby the NE2 nitrogen is directed at one or the other hydroxyl group within the crystal. In contrast, the yeast structure containing BMP is modeled with the CE1 carbon of the analogous histidine (rather than the NE2 nitrogen) directed toward the ribose hydroxyls; no hydrogen bonds as modeled. Scrutiny of this model by the structure validation server, MOLPROBITY (*34*) suggests that this histidine is modeled incorrectly. In any case, an asparagine residue would be better able to form multiple hydrogen bonds than a histidine at this position. The bacterial enzymes have a glycine at this position, although bifurcated hydrogen bonds to the ribose hydroxyls are contributed by a water molecule. Another difference is that the human/yeast enzymes have an additional serine hydrogen bonding the 3′-hydroxyl of the ribose (Figures 4c and 5, S257). This residue is replaced by a glycine residue in the malarial structures (G21, or an alanine in most prokaryotic structures), and a water molecule (Figure 4c, red sphere) makes the analogous hydrogen bond.

Binding of XMP and Differential Inhibition. For ODCase structures complexed with UMP, AzaUMP, or BMP, the

pyrimidine rings slot into the narrow hydrophobic cleft of the active site. Despite its larger size, XMP is a potent competitive inhibitor of ODCase (Table 1). There are only two structures of XMP complexes, the *Pyrococcus* and *Methanobacterium* ODCases. In both cases, the purine rings are in the anti-conformation and do not fully enter the cleft normally occupied by a pyrimidine ring. In the *Methanobacterium* structure, this is due to a molecule of 1,3-butanediol residing in the pyrimidine ring pocket. In the *Pyrococcus* structure, XMP is positioned differently in the A- and B-subunits. In the B-subunit, XMP is positioned as for the *Methanobacterium* structure, although 4 water molecules reside in the pyrimidine binding pocket. In the A-subunit, the purine ring is more deeply inserted in the pyrimidine cleft and slightly twisted with respect to UMP (Figure 4d). The phosphate-binding loop is disordered in the A-subunit and closed in the B-subunit despite XMP being less deeply inserted. In both active sites, XMP binding is accommodated by an expansion of the cleft (between the subunits), which accepts the aromatic ring (note the movement of helices α2 and α3 and the βα5-loop in Figure 4d).

The different manner in which *Pyrococcus* ODCase binds UMP and XMP not only concerns the positions of the aromatic rings and phosphate-binding loop but also extends to the phosphoribosyl group of the ligands (Figure 4d). In both A- and B-subunits, the ribose of XMP is unable to directly hydrogen bond to the asparagine residue as observed for the UMP-complexes of *Pyrococcus* and malarial ODCases (N104 in Figure 4c). In the XMP-*Pyrococcus* structure, an alternate rotamer of the asparagine is adopted, which hydrogen bonds the 2′-hydroxyl of the ribose via a bridging water molecule (Figure 4d, dashed lines and red sphere). Although the positions of the ribose group of XMP, bridging water, and asparagine are different in the A- and B-subunits, they interact in a similar manner. Last, both subunits of both complexes contain similarly positioned phosphate groups of the UMP and XMP ligands.

DISCUSSION

PfODCase Characterization and Kinetic Analysis of Inhibitors. Recombinant *Pf*ODCase has been analyzed by size-exclusion chromatography and analytical ultracentrifugation and found to be a stable homodimer of ~76 kDa in solution, consistent with monomer masses obtained by mass spectrometry and calculated theoretically, and consistent with the crystal structure discussed below. The apparent K_m of OMP for recombinant *Pf*ODCase (350 ± 60 nM, Table 1) is ~0.1-fold the value reported for *Pf*ODCase purified directly from the parasite (K_m ~ 3200 nM) (*36*) and equivalent to values obtained for the human (K_m~ 295 nM) (*37*) and yeast (K_m ~ 700 nM) (*11*) enzymes. The V_{max} of 2.70 ± 0.10 μmol/min/mg protein obtained for *Pf*ODCase is equivalent to a turnover number of 1.7 s^{-1}, compared with a value of 5 s^{-1} from our previous work (*24*) and 15.6 s^{-1} obtained for ODCase purified directly from *P. falciparum* (*36*). The present turnover number of 1.7 s^{-1} was obtained with a sensitive radioassay to measure true initial reaction velocities from the conversion of only 5% of the OMP to UMP. The latter two values were obtained using a relatively insensitive spectrophotomeric assay that follows the decrease in absorbance at 285 nm. In addition, there may be some minor structural difference between the recombinant *Pf*ODCase and the native enzyme.

A number of nucleoside 5′-monophosphate analogues, including AzaUMP, Pyrazofurin 5′-monophosphate, BMP, allopurinol-3-riboside 5′-monophosphate, and XMP, have been reported as inhibitors of various ODCases. The K_i value of AzaUMP for human ODCase is ~510 nM (*38*) compared with that of the yeast enzyme (~64 nM) (*11*) and *Pf*ODCase determined here (K_i = 12 ± 3 nM, Table 1). Thus, AzaUMP is an ~43-fold more potent inhibitor of *Pf*ODCase compared with the human enzyme (Table 1). The K_i value of allopurinol-3-riboside 5′-monophosphate for the human erythrocytic ODCase is ~2600 nM (*37*) compared with those of the yeast enzyme (~1000 nM) (*11*) and *Pf*ODCase determined here (K_i = 240 ± 20 nM). Hence, allopurinol-3-riboside 5′-monophosphate is an 11-fold more potent inhibitor of *Pf*ODCase compared with the human enzyme (Table 1). Pyrazofurin 5′-monophosphate is a potent inhibitor of yeast ODCase (K_i ~5 nM) (*39*) and *P. falciparum* determined here (K_i = 3.6 ± 0.7 nM), with no value available for the human enzyme. Pyrazofurin 5′-monophosphate has approximately equivalent inhibitory effects on yeast and malarial ODCases (Table 1). The purine nucleotide XMP inhibits human ODCase (K_i ~ 670 nM) (*37*), the yeast enzyme (K_i ~ 410 nM) (*11*), and *Pf*ODCase determined here (K_i = 4.4 ± 0.7 nM). Poduch et al. (*40*) recently reported a K_i value for XMP of 43 ± 2 nM for the inhibition of *Pf*ODCase. Their assay used an isothermal titration calorimeter that would lack the sensitivity of the radioassay used in the present work (Table 1), where true initial reaction velocities were measured. Thus, XMP is an ~150-fold more potent inhibitor of *Pf*ODCase compared with the human enzyme (Table 1), compared with 43-fold for AzaUMP. In contrast, allopurinol-3-riboside 5′-monophosphate and Pyrazofurin 5′-monophosphate do not show such differential inhibition. Elucidation of the structures of human and malarial ODCase-XMP complexes could provide an explanation of the major difference in inhibition observed for XMP, providing a basis for the development of antimalarial drugs. BMP is also a potent inhibitor of *Pf*ODCase (data not shown), as for the human and yeast enzymes (*41*). However, a detailed kinetic analysis will be required to determine the mechanism of inhibition and a dissociation constant.

Structure of Malarial ODCase. Despite performing numerous crystallization trials involving *Pf*ODCase with UMP, AzaUMP, or XMP, only a single crystal, grown in the absence of ligand, was obtained. The structure was solved by molecular replacement using PDB coordinates recently deposited by the Structural Genomics of Pathogenic Protozoa Consortium (SGPP; http://www.sgpp.org/). The classic TIM-barrel fold of our structure (Figure 3a) differs from this pre-existing *Pf*ODCase structure in one of its 8 segments: the end of the β5-strand and the adjacent βα5-loop (Figure 3a, magenta ribbon, and Figure 3b). On the basis of the positions of residues in this segment, implicated by amino acid and structural homology to be important for catalysis, we propose that our structure represents a more active conformation (*Pf*ODCase-act) where the pyrimidine-binding end of the active site pocket is fully formed. In contrast, the more open active site of the pre-existing *Pf*ODCase structures (PDB codes 2F84 and 2Q8L) may represent a ground-state or resting conformation (*Pf*ODCase-rest). This conclusion is

supported by superposing our structure with those of other *Plasmodium* species (*P. vivax*, *P. yoelii*, and *P. berghei*; Figure 3c)[3]. The structural homology between the active-βα5-loop forms of the malarial ODCases is high, particularly at the active site, even though the *P. yoelii* enzyme contains a bound sulfate ion, the *P. berghei* enzyme contains an iodide ion, and the structures of the *P. vivax* enzyme contain UMP or AzaUMP. An additional difference noted between the malarial ODCases concerns the conformation of the phosphate binding loop: closed for the two *P. vivax* and single *P. yoelii* structures (containing UMP, AzaUMP, or sulfate, respectively) but in open or disordered conformations for the *Pf*ODCase structures. The malarial ODCases differ from those of other species by an additional ~55 residues in the βα1-loop, increased size of the βα5-loop (which is dynamic in the case of *Pf*ODCase), and variability in the size and conformation of the phosphate-binding loop.

Loop Dynamics. The phosphate-binding loop and the βα5-loop can adopt multiple conformations. The phosphate-binding loop in our *Pf*ODCase structure is ordered in the A-subunit and disordered in the B-subunit, probably because of different packing within the crystal lattice. Alternate crystal contacts may indirectly influence the different solvent networks observed in the two active sites despite some of these differentially positioned waters being deep in the active site cleft and out of contact with bulk solvent or the phosphate-binding loop (Figure 4b). An asymmetric distribution of waters also exists in the *P. berghei* structure. The observation of unique waters in ostensibly identical environments suggests that the displacement of solvent required for the binding of substrate is easily achieved by even the slightest of conformational changes, which no doubt accompany substrate binding.

The phosphate-binding loop plays a key role in stabilizing the enzyme−ligand complex. As evident from the many ODCase structures listed in Table 3, this loop is generally observed in a closed conformation over bound product or analogue or is open or disordered in the absence of ligand. An invariant glutamine residue in this loop (Q269 in *Pf*ODCase) (*35*) provides hydrogen bonding to one oxygen on the phosphate and also to the C2 oxygen of the product UMP (*14, 20*) or of the inhibitors azaUMP (*20*) and BMP (*12, 13*) (Figure 5). The fact that Q269 normally binds to two atoms far apart on the nucleotide may account for the inability of bound phosphate or iodide ions alone to close the loop (Table 3).

The βα5-loop dynamics observed in the *Pf*ODCase structures have not been observed for other ODCases. The *Pf*ODCase structures have different conformations of this loop, only one of which lines the pyrimidine-binding cleft as might be expected for catalysis (Figure 3b). The *Pf*ODCase-rest structures were crystallized in a different space group and unit cell to our *Pf*ODCase-act structure. The βα5-loop in these resting-βα5-loop structures interacts with the corresponding loop from the dimer partner and with a helix presented by a neighboring (nondimer partner) molecule. These crystal contacts are absent in the *Pf*ODCase-act structure (see Supporting Information, Figure S1). The alternate conformations observed for the βα5-loop (and phosphate-binding loop) may result solely from different crystal packing environments and be irrelevant to ODCase in solution. However, the frequency with which TIM-barrel enzymes display loop-in/out variability, often affecting active sites, suggests that the conformations of *Pf*ODCase observed could indeed represent *bona fide* intermediates along the reaction pathway between substrate binding and product release (*43, 44*).

As the βα5-loop is part of the dimerization interface, structural rearrangement occurring in one subunit is mirrored by the dimer partner, providing a potential mechanism for cooperativity between the active sites. Binding of OMP to one loop-out subunit may induce local loop-in movement, with a conformational change in the other subunit. However, cooperativity with respect to OMP has not been reported for ODCase. In an extensive review of ODCases, Miller and Wolfenden (*11*) discussed the paradox that although competitive inhibitors of ODCase display a wide range of inhibition constants, they often bind in a near-identical manner. They suggested that ODCases might be capable of active-site rearrangements or conformations yet to be observed crystallographically. Perhaps the βα5-loop conformations observed for *Pf*ODCase are an example of such dynamics that might be at play in the reaction pathways of all ODCases.

Catalytic Mechanism and Differential Inhibition by XMP. The catalytic mechanism of ODCase remains undefined, although numerous mechanisms have been proposed (*11*). The arrangement of residues that line the active site of the present *Pf*ODCase structure is similar to that of other ODCases (*Pf*ODCase and human ODCase are juxtaposed in Figure 5). Without structures of human and malarial ODCases complexed with XMP, rationalization of the differential binding of XMP is difficult. Some differences between the active sites include the size and disposition of the phosphate-binding loop and the identities of several amino acids whose side chains are positioned to hydrogen bond with the ribose-hydroxyls of UMP or an analogue. Residues N104 and G21 of the malarial structures are replaced by H283 and S257 in the human structure (Figures 4c and 5). More minor differences between human and malarial enzymes include the conservative substitution of several residues of the βα5-loop (T195 replaced by S372 and N196 replaced by S373), and a methionine residue projecting from the βα5-loop (M371) of the human enzyme is replaced by $M168^{B}$ from the B-subunit of the malarial enzyme (Figure 5).

The phosphate-binding loop of human ODCase is considerably larger than that for the malarial enzymes and would probably require repositioning to enable XMP to bind in either of the modes observed for the *Pyrococcus*-XMP structure (Figure 4d). The phosphate-binding loop of the malarial enzymes is the same size and shape as the *Pyrococcus* loop and may behave similarly, although it is

[3] Our conclusion is also supported by low resolution *Pf*ODCase structures published by Tokuoka et al., just prior to the submission of this manuscript (*42*). PDB codes 2ZA2, 2ZA1, and 2ZA3, all at ~2.65 Å resolution and comprising apo, OMP-, and UMP-complexed *Pf*ODCase, also have the βα5-loop in the active conformation. The apo enzyme has disordered phosphate-binding loops, while in the OMP and UMP complexes, they are closed. The OMP and UMP ligands overlay almost perfectly with the UMP ligand modeled in Figures 3 and 4 of this article. The carboxylate moiety of OMP is accommodated by a subtle rotation of the side chain of D136. In contrast, other fine-detail features, such as the expected bifurcated hydrogen-bonding between Q269 and substrate/product, are not apparent in these lower resolution structures.

unclear whether the loop would be ordered or disordered in the presence of XMP. Another similarity shared between the malarial and *Pyrococcus* structures is the presence of an asparagine (N104, Figure 4c) positioned to hydrogen bond the ribose-hydroxyls of the ligand. In the presence of XMP, a different conformation of N104 contacts a differently positioned ribose group via a bridging water molecule. The same alternate rotamer may be used when *Pf*ODCase binds XMP. The histidine which substitutes for this residue in the human enzyme might interact with the ribose in a different manner or not at all. Although XMP is shown to bind the *Pyrococcus* and *Methanobacterium* enzymes in the anti-conformation, considerable rotation about the glycosidic bond is possible for this nucleotide (*45*) and may account for its ability to differentially inhibit ODCases from disparate organisms. In contrast, UMP, which has the poorest K_i of the inhibitors assayed (Table 1), in solution predominantly adopts the syn-conformation (*45*), as opposed to the anti-conformation observed in the ODCase crystal structures, possibly explaining its weak potency as an ODCase inhibitor. While obtaining crystals of both enzymes complexed with XMP may ultimately explain the differential inhibition by XMP, the human and malarial ODCase structures available provide a starting point for the rational design of more specific *Pf*ODCase inhibitors.

ACKNOWLEDGMENT

We thank Dr. Lakshmi Kotra (University of Toronto, Canada) for providing BMP and Dr. Ben Crossett (Australian Proteome Analysis Facility, Sydney, Australia) for mass spectrometry.

SUPPORTING INFORMATION AVAILABLE

Figure S1 illustrates the different crystal contacts observed in our *Pf*ODCase structure and those observed in PDB codes 2F84 and 2Q8L. This material is available free of charge via the Internet at http://pubs.acs.org.

REFERENCES

1. Gardner, M. J., Hall, N., Fung, E., White, O., Berriman, M., Hyman, R. W., Carlton, J. M., Pain, A., Nelson, K. E., Bowman, S., Paulsen, I. T., James, K., Eisen, J. A., Rutherford, K., Salzberg, S. L., Craig, A., Kyes, S., Chan, M. S., Nene, V., Shallom, S. J., Suh, B., Peterson, J., Angiuoli, S., Pertea, M., Allen, J., Selengut, J., Haft, D., Mather, M. W., Vaidya, A. B., Martin, D. M., Fairlamb, A. H., Fraunholz, M. J., Roos, D. S., Ralph, S. A., McFadden, G. I., Cummings, L. M., Subramanian, G. M., Mungall, C., Venter, J. C., Carucci, D. J., Hoffman, S. L., Newbold, C., Davis, R. W., Fraser, C. M., and Barrell, B. (2002) Genome sequence of the human malaria parasite *Plasmodium falciparum*. *Nature 419*, 498–511.
2. Nchinda, T. C. (1998) Malaria: a reemerging disease in Africa. *Emerging Infect. Dis. 4*, 398–403.
3. Van Dyke, K., Tremblay, G. C., Lantz, C. H., and Szustkiewicz, C. (1970) The source of purines and pyrimidines in *Plasmodium berghei*. *Am. J. Trop. Med. Hyg. 19*, 202–208.
4. Sherman, I. W. (1979) Biochemistry of *Plasmodium* (malarial parasites). *Microbiol. Rev. 43*, 453–495.
5. Scheibel, L. W., and Scherman, I. W. (1988) *Malaria: Principles and Practice of Malariology,* (Wernsdorfer, W. H., and McGreggor, I., Eds.) pp 234–242, Churchill Livingstone, London.
6. Floyd, E. E., and Jones, M. E. (1985) Isolation and characterization of the orotidine 5′-monophosphate decarboxylase domain of the multifunctional protein uridine 5′-monophosphate synthase. *J. Biol. Chem. 260*, 9443–9451.
7. Jones, M. E. (1980) Pyrimidine nucleotide biosynthesis in animals: genes, enzymes, and regulation of UMP biosynthesis. *Annu. Rev. Biochem. 49*, 253–279.
8. Livingstone, L. R., and Jones, M. E. (1987) The purification and preliminary characterization of UMP synthase from human placenta. *J. Biol. Chem. 262*, 15726–15733.
9. Yablonski, M. J., Pasek, D. A., Han, B. D., Jones, M. E., and Traut, T. W. (1996) Intrinsic activity and stability of bifunctional human UMP synthase and its two separate catalytic domains, orotate phosphoribosyltransferase and orotidine-5′-phosphate decarboxylase. *J. Biol. Chem. 271*, 10704–10708.
10. Radzicka, A., and Wolfenden, R. (1995) A proficient enzyme. *Science 267*, 90–93.
11. Miller, B. G., and Wolfenden, R. (2002) Catalytic proficiency: the unusual case of OMP decarboxylase. *Annu. Rev. Biochem. 71*, 847–885.
12. Harris, P., Poulsen, J. C., Jensen, K. F., and Larsen, S. (2002) Substrate binding induces domain movements in orotidine 5′-monophosphate decarboxylase. *J. Mol. Biol. 318*, 1019–1029.
13. Harris, P., Navarro Poulsen, J. C., Jensen, K. F., and Larsen, S. (2000) Structural basis for the catalytic mechanism of a proficient enzyme: orotidine 5′-monophosphate decarboxylase. *Biochemistry 39*, 4217–4224.
14. Appleby, T. C., Kinsland, C., Begley, T. P., and Ealick, S. E. (2000) The crystal structure and mechanism of orotidine 5′-monophosphate decarboxylase. *Proc. Natl. Acad. Sci. U.S.A. 97* 2005–2010.
15. Miller, B. G., Snider, M. J., Short, S. A., and Wolfenden, R. (2000) Contribution of enzyme-phosphoribosyl contacts to catalysis by orotidine 5′-phosphate decarboxylase. *Biochemistry 39*, 8113–8118.
16. Miller, B. G., Hassell, A. M., Wolfenden, R., Milburn, M. V., and Short, S. A. (2000) Anatomy of a proficient enzyme: the structure of orotidine 5′-monophosphate decarboxylase in the presence and absence of a potential transition state analog. *Proc. Natl. Acad. Sci. U.S.A. 97*, 2011–2016.
17. Wu, N., and Pai, E. F. (2002) Crystal structures of inhibitor complexes reveal an alternate binding mode in orotidine-5′-monophosphate decarboxylase. *J. Biol. Chem. 277*, 28080–28087.
18. Wu, N., and Pai, E. F. (2004) Crystallographic studies of native and mutant orotidine 5′ phosphate decarboxylases. *Top. Curr. Chem. 238*, 23–42.
19. Wu, N., Mo, Y., Gao, J., and Pai, E. F. (2000) Electrostatic stress in catalysis: structure and mechanism of the enzyme orotidine monophosphate decarboxylase. *Proc. Natl. Acad. Sci. U.S.A. 97*, 2017–2022.
20. Wu, N., Gillon, W., and Pai, E. F. (2002) Mapping the active site-ligand interactions of orotidine 5′-monophosphate decarboxylase by crystallography. *Biochemistry 41*, 4002–4011.
21. Jencks, W. P. (1975) Binding energy, specificity, and enzymic catalysis: the circe effect. *Adv. Enzymol. Relat. Areas Mol. Biol. 43*, 219–410.
22. Christopherson, R. I., Lyons, S. D., and Wilson, P. K. (2002) Inhibitors of de novo nucleotide biosynthesis as drugs. *Acc. Chem. Res. 35*, 961–971.
23. Cinquin, O., Christopherson, R. I., and Menz, R. I. (2001) A hybrid plasmid for expression of toxic malarial proteins in *Escherichia coli*. *Mol. Biochem. Parasitol. 117*, 245–247.
24. Menz, R. I., Cinquin, O., and Christopherson, R. I. (2002) The identification, cloning and functional expression of the gene encoding orotidine 5′-monophosphate (OMP) decarboxylase from *Plasmodium falciparum*. *Ann. Trop. Med. Parasitol. 96*, 469–476.
25. Bradford, M. M. (1976) A rapid and sensitive method for the quantitation of microgram quantities of protein utilizing the principle of protein-dye binding. *Anal. Biochem. 72*, 248–254.
26. Rawls, J. M., Jr. (1978) Enzymatic synthesis of [6–14C]orotidine 5′-monophosphate and its use in the assay of orotate phosphoribosyltransferase and orotidylate decarboxylase. *Anal. Biochem. 86*, 107–117.
27. Fyfe, J. A., Keller, P. M., Furman, P. A., Miller, R. L., and Elion, G. B. (1978) Thymidine kinase from herpes simplex virus phosphorylates the new antiviral compound, 9-(2-hydroxyethoxymethyl)guanine. *J. Biol. Chem. 253*, 8721–8727.
28. Brusilow, S. W., and Hauser, E. (1989) Simple method of measurement of orotic acid and orotidine in urine. *J. Chromatogr. 493*, 388–391.
29. Otwinowski, Z., and Minor, W. (1997) Processing of X-ray diffraction data collected in oscillation mode. *Methods Enzymol. 276*, 307–326.
30. Vagin, A., and Teplyakov, A. (1997) MOLREP: an automated program for molecular replacement. *J. Appl. Crystallogr. 30*, 1022–1025.
31. Lamzin, V. S., and Wilson, K. S. (1993) Automated refinement of protein models. *Acta Crystallogr., Sect. D 49*, 129–147.

32. Emsley, P., and Cowtan, K. (2004) Coot: model-building tools for molecular graphics. *Acta Crystallogr., Sect. D 60*, 2126–2132.
33. Lee, B., and Richards, F. M. (1971) The interpretation of protein structures: estimation of static accessibility. *J. Mol. Biol. 55*, 379–400.
34. Lovell, S. C., Davis, I. W., Arendall, W. B., III, de Bakker, P. I., Word, J. M., Prisant, M. G., Richardson, J. S., and Richardson, D. C. (2003) Structure validation by Calpha geometry: phi,psi and Cbeta deviation. *Proteins 50*, 437–450.
35. Traut, T. W., and Temple, B. R. (2000) The chemistry of the reaction determines the invariant amino acids during the evolution and divergence of orotidine 5′-monophosphate decarboxylase. *J. Biol. Chem. 275*, 28675–28681.
36. Krungkrai, S. R., Prapunwattana, P., Horii, T., and Krungkrai, J. (2004) Orotate phosphoribosyltransferase and orotidine 5′-monophosphate decarboxylase exist as multienzyme complex in human malaria parasite *Plasmodium falciparum*. *Biochem. Biophys. Res. Commun. 318*, 1012–1018.
37. Brown, G. K., and O'Sullivan, W. J. (1977) Inhibition of human erythrocyte orotidylate decarboxylase. *Biochem. Pharmacol. 26*, 1947–1950.
38. Miller, B. G., Traut, T. W., and Wolfenden, R. (1998) Effects of substrate binding determinants in the transition state for orotidine 5′-monophosphate decarboxylase. *Bioorg. Chem. 26*, 283–288.
39. Dix, D. E., Lehman, C. P., Jakubowski, A., Moyer, J. D., and Handschumacher, R. E. (1979) Pyrazofurin metabolism, enzyme inhibition, and resistance in L5178Y cells. *Cancer Res. 39*, 4485–4490.
40. Poduch, E., Wei, L., Pai, E. F., and Kotra, L. P. (2007) Structural diversity and plasticity associated with nucleotides. *J. Med. Chem.*, in press.
41. Levine, H. L., Brody, R. S., and Westheimer, F. H. (1980) Inhibition of orotidine-5′-phosphate decarboxylase by 1-(5′-phospho-beta-d-ribofuranosyl)barbituric acid, 6-azauridine 5′-phosphate, and uridine 5′-phosphate. *Biochemistry 19*, 4993–4999.
42. Tokuoka, K., Kusakari, Y., Krungkrai, S. R., Matsumura, H., Krungkrai, J., Horii, T., and Inoue, T. (2007) Structural basis for the decarboxylation of orotidine 5′-monophosphate (OMP) by *Plasmodium falciparum* OMP decarboxylase. *J. Biochem.*, *143*, 69–78.
43. Lee, M., Chan, C. W., Mitchell Guss, J., Christopherson, R. I., and Maher, M. J. (2005) Dihydroorotase from *Escherichia coli*: loop movement and cooperativity between subunits. *J. Mol. Biol. 348*, 523–533.
44. Langley, D. B., Harty, D. W. S., Jacques, N. A., Hunter, N., Guss, J. M., and Collyer, C. A. (2008) Structure of N-acetyl-β-D-glucosaminidase (GcnA) from the endocarditis pathogen *Streptococcus gordonii* and its complex with the mechanism-based inhibitor NAG-thiazoline. *J. Mol. Biol.*, in press.
45. Saenger, W., Suck, D., Knappenberg, M., and Dirkx, J. (1979) Theoretical drug design: 6-azauridine-5′-phosphate--its X-ray crystal structure, potential energy maps, and mechanism of inhibition of orotidine-5′-phosphate decarboxylase. *Biopolymers 18*, 2015–2036.

BI702390K